Molecular BioSystems

PAPER

View Article Online
View Journal

Extracellular matrix density promotes EMT by weakening cell–cell adhesions†

Cite this: DOI: 10.1039/c3mb70431a

Sandeep Kumar, Alakesh Das and Shamik Sen*

Epithelial to mesenchymal transition (EMT), the process during which epithelial cells lose adhesions with neighbouring cells and get converted to migratory and invasive cells, is closely tied to cancer progression. Cancer progression is also marked by increased deposition and cross linking of fibrillar extracellular matrix (ECM) proteins including collagen and fibronectin, which lead to increase in ECM density and increased cell–matrix adhesions. Thus, an imbalance between cell–matrix and cell–cell adhesions underlies cancer progression. Though several experimental studies have shown a crosstalk between cell–cell and cell–matrix adhesions, the extent to which changes in ECM density can trigger EMT *via* formation of cell–matrix adhesions and disassembly of cell–cell adhesions remains incompletely understood. In this paper, we have developed a computational framework for studying modulation of cell–cell adhesion by ECM density, integrating findings from multiple studies that connect ECM-mediated adhesion signaling and growth factor signaling with cell–cell adhesion. Here, we have specifically tracked changes in the levels of the E-cadherin–β catenin (Eβ) complex in response to alterations in ECM density. Our results illustrate a tug-of-war between ECM density and E-cadherin in determining Eβ levels both for a single cell as well as for a cell population, with increase in ligand density weakening cell–cell adhesions and increase in E-cadherin levels counterbalancing the effect of ECM density. Consistent with model predictions, lower levels of membrane to cytoplasmic ratios of E-cadherin were observed in MCF-7 human breast cancer cells plated on substrates with increasing collagen density. By performing simulations for a heterogeneous population consisting of both normal and EMT cells, we demonstrate that ligand density and the fraction of EMT cells collectively determine the scattering potential of a cell population. Taken together, our findings are in support of a model where increase in cell–matrix adhesions negatively regulates cell–cell adhesions thereby contributing to EMT and enhanced cellular invasion.

Received 26th September 2013,
Accepted 10th January 2014

DOI: 10.1039/c3mb70431a

www.rsc.org/molecularbiosystems

1 Introduction

Epithelial to mesenchymal transition (EMT) plays a key role both in embryogenesis and in carcinogenesis.[1,2] In the case of the latter, EMT has been associated with cancer invasion, metastasis, drug resistance and poor clinical outcome.[3] EMT is generally induced by cytokines like TGF-β, which in turn activate several signaling pathways ultimately repressing the expression of the cell–cell adhesion molecule E-cadherin.[4] Cell–cell adhesion is maintained by the E-cadherin–β-catenin complex (Eβ complex in short), where the extracellular domain of E-cadherin of one cell binds to the extracellular domain of E-cadherin of its neighbouring cell, and the cytoplasmic E-cadherin tail links to the cytoskeleton *via* the protein β-catenin.[5,6] The strength of cell–cell adhesions is directly determined by the concentration of the Eβ complex at the cell membrane.[7,8] Cell–cell adhesion can be weakened either by downregulating E-cadherin or by phosphorylating β-catenin. Upon breakage of cell–cell adhesions, both E-cadherin and β-catenin translocate to the cytoplasm.[5]

The extracellular matrix (ECM), that undergoes drastic alterations in composition and organization during cancer progression, contributes to cell invasion in both EMT-dependent and EMT-independent manners. The tumor stroma is enriched in fibrillar proteins like collagen I and fibronectin, and undergoes reorganisation from a random network to an aligned network *via* LOX-mediated collagen crosslinking.[9,10] Such remodelling is associated with ECM stiffening and has been directly implicated in cancer progression.[11,12] In breast cancer, the tumor microenvironment undergoes a nearly 10–20 fold increase in bulk stiffness, reaching a value of 4 kPa. Even in the absence of any soluble cues, such stiffening has been shown to be capable of disrupting acinar morphology of mammary epithelial cells,

WRCBB, Department of Biosciences and Bioengineering, IIT Bombay, Mumbai, India. E-mail: shamiks@iitb.ac.in

† Electronic supplementary information (ESI) available. See DOI: 10.1039/c3mb70431a

via enhanced integrin clustering, FAK phosphorylation, RhoA activation and increased cellular contractility. Further, the cross linking mediated tensing of individual ECM fibers may expose and activate soluble factors like TGF-β[13] which further contribute to cellular invasion by triggering EMT. Independent of stiffening effects, increase in ECM density *via* crosslinking may also contribute to increased extracellular proteolysis through modulation of myosin-based contractility.[14]

Though cell–cell adhesions are required for maintaining the integrity of epithelial cells, and cell–matrix adhesions are present in mesenchymal cells, several studies have demonstrated a crosstalk between these two types of adhesions.[15] Interestingly, in a range of different cell-types including squamous cell carcinoma and cadherin-expressing L fibroblasts, integrin ligation led to an increase in cell–cell adhesion measured using a dual pipette assay.[16] In direct contrast, when cancer cells were cultured on micropatterned substrates coated with a combination of cadherins and ECM proteins, the formation of cell–matrix adhesions prevented the formation of cell–cell adhesions.[17] In the case of epithelial cells, deposition of ECM proteins on top of an epithelial monolayer has been shown to cause a re-distribution of cell–cell adhesions from the top ECM-rich zone to the bottom ECM-free zone.[18] Such negative feedback has also been observed in vascular smooth muscle cells cultured at high density, wherein concomitant with the formation of cell–cell adhesions, there was a corresponding decrease in the expression of focal adhesion proteins talin and vinculin.[19] Of the several signaling cascades regulating the crosstalk between cell–cell and cell–matrix adhesions,[20–23] one of the well characterized pathways involves FAK mediated phosphorylation of β-catenin *via* the FAK → Grb2 → Dvl → Rac → JNK cascade.[24] Upon integrin clustering, FAK gets activated, activates the adaptor protein Grb2, and increases the synergy between Dvl and Grb2. Grb2 and Dvl in turn activate the Rac GTPase, which enhances JNK activation.[25] Upon activation, JNK phosphorylates β-catenin at Ser191 and Ser605 sites leading to disassembly of the Eβ complexes.[6]

Mathematical modeling approaches have contributed significantly to our understanding of cancer and related processes.[26–29] While ODE and PDE-based continuous models are widely used for studying dynamics of continuous quantities, discrete models (*e.g.*, cellular automata, lattice based model, agent based models) are more suitable for studying dynamics of population of cells. Of these, cellular automaton (CA) provides a computational framework in which population is divided into automaton cells and each cell evolved in time as per some defined rule(s).[30] CA has received particular attention because of its ability to generate a wide range of patterns that arise from such simple rules and can recapitulate many features of complex biological systems. Consequently, CA has been used to model various aspects of cancer including tumor growth,[31] role of ECM fiber-crosslinking on ECM degradation,[32] cancer stem cell proliferation,[33] tumor–stroma interaction in prostate cancer[34] and influence of fibroblasts in melanoma.[35]

In this paper, we have developed a mathematical model for exploring the crosstalk between cell–cell and cell–matrix adhesions during tumorigenesis. Specifically, we have varied cell–matrix adhesions by varying ligand density and have quantified cell–cell adhesion based on the concentration of the Eβ complex. Consistent with experiments, our results demonstrate that upregulation in ligand density promotes EMT *via* weakening of cell–cell adhesions. This effect can be partly reversed by overexpression of E-cadherin. The model was further extended using a cellular automata framework to study population-level Eβ dynamics taking cell–cell crosstalk into account. By varying ligand density and the fraction of cells that have already undergone EMT (*i.e.*, have very low E-cadherin expression), we have demonstrated the collective influence of ligand density and the fraction of EMT cells on population-level scattering. Similar results were observed experimentally in the E-cadherin localization patterns in MDA-MB-231 and MCF-7 breast cancer cells when plated on substrates with increasing collagen I density. Taken together, our results demonstrate the complex interplay between cell–matrix and cell–cell adhesions in determining the scattering potential of a cell population. The computational framework developed in this paper can be further extended for studying how these variables regulate other morphogenetic processes including cell sorting and collective cell migration.

2 Materials and methods

Regulation of cell–cell adhesion by ECM density: a unified model

Several studies have demonstrated the influence of ECM density on cell–cell adhesions *via* multiple pathways. Although, the exact mechanisms governing the propagation of signals from cell–ECM adhesion to cell–cell adhesion are not completely known, several independent reports establish links between individual molecules. For understanding the influence of ECM density on cell–cell adhesion, a model was developed based on the following signaling events:

(1) Increase in ECM density increases FAK activity.[36]

(2) Increase in FAK activity increases Grb2 activity.[24]

(3) Activated Grb2 drives Dvl-mediated activation of Rac.[24]

(4) Increase in Rac increases the concentration of activated JNK.[24]

(5) JNK phosphorylates β-catenin.[6]

(6) Non-phosphorylated β-catenin complexes with membrane bound E-cadherin (E_c) to form a E-cadherin–β-catenin bond (Eβ) which facilitates cell–cell adhesion.[5]

(7) The Eβ complex dissociates into E-cadherin and β-catenin.[5]

The schematic representation of the proposed network, based on the above-mentioned kinetic activities, is shown in Fig. 1. In addition, protein degradation was also taken into account. For studying the dynamics of the network, the kinetic events were converted into the following chemical kinetic equations:

$$[\mathrm{FAK}] \xrightarrow{k_1,[\mathrm{L}]} [\mathrm{FAK}^*] \quad (1)$$

$$[\mathrm{GRB2}] \xrightarrow{k_2,[\mathrm{FAK}^*]} [\mathrm{GRB2}^*] \quad (2)$$

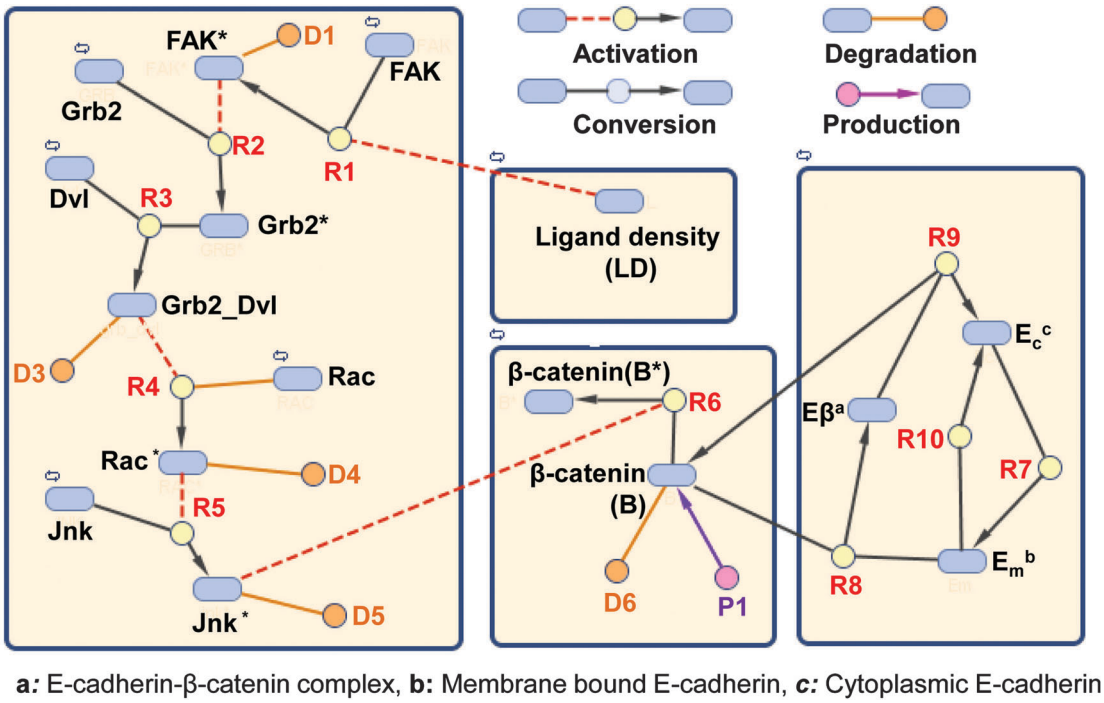

Fig. 1 Model of ECM density-dependent modulation of cell–cell adhesion. Signaling network through which ECM density modulates cell–cell adhesion. Upon integrin engagement with the ECM ligand, FAK gets activated and subsequently activates the adaptor protein Grb2. Activated Grb2 protein synergizes with Dvl protein and causes JNK phosphorylation through Rac activation. Activated JNK phosphorylates β-catenin thereby reducing the rate of cell–cell adhesion formation. Solid lines represent formation/disruption of the complex. Dotted lines represent protein activation (*e.g.*, phosphorylation). Refer to Materials and methods for further details.

$$[\mathrm{GRB2}^*] + [\mathrm{DVL}] \xrightarrow{k_3} [\mathrm{GRB2\_DVL}] \quad (3)$$

$$[\mathrm{RAC}] \xrightarrow{k_4,[\mathrm{GRB2\_DVL}]} [\mathrm{RAC}^*] \quad (4)$$

$$[\mathrm{JNK}] \xrightarrow{k_5,[\mathrm{RAC}^*]} [\mathrm{JNK}^*] \quad (5)$$

$$[\beta] \xrightarrow{k_6,[\mathrm{JNK}^*]} [\beta^*] \quad (6)$$

$$[\beta] + [E_\mathrm{m}] \xrightarrow{k_8} [\mathrm{E}\beta] \quad (7)$$

$$[E_\mathrm{c}] \xrightarrow{k_7,E_\mathrm{m},\beta} [E_\mathrm{m}] \quad (8)$$

$$[E_\mathrm{m}] \xrightarrow{k_{10},\mathrm{E}\beta} [E_\mathrm{c}] \quad (9)$$

$$[\mathrm{E}\beta] \xrightarrow{k_9} [\beta] + [E_\mathrm{c}] \quad (10)$$

These kinetic reactions were transformed into an ordinary differential equation (ODE)-based continuous deterministic model to study the influence of ECM density on cell–cell adhesion (see next section). The coupled-ODE based model was then solved using Matlab. To verify the model solution obtained from Matlab, the SimBiology toolbox of Matlab was used to directly simulate the signaling network shown in Fig. 1. The details of the mathematical models, values of reaction constants, and initial concentrations of all proteins are discussed in the next section.

Mathematical model of a single cell

For developing the ODE model of a single cell, the 10 biochemical reactions (eqn 1 to 10) were codified into the following 9 differential equations (eqn 11 to 19), with each differential equation representing the dynamics of an individual protein:

$$\frac{\mathrm{d}[\mathrm{FAK}^*]}{\mathrm{d}t} = k_1 \times \frac{[\mathrm{LD}]}{C + [\mathrm{LD}]} \times [\mathrm{FAK}] - d_1 \times [\mathrm{FAK}^*] \quad (11)$$

$$\frac{\mathrm{d}[\mathrm{Grb2}^*]}{\mathrm{d}t} = k_2 \times [\mathrm{FAK}^*][\mathrm{Grb2}] - k_3 \times [\mathrm{Grb2}^*][\mathrm{Dvl}] \quad (12)$$

$$\frac{\mathrm{d}[\mathrm{Grb2\_Dvl}]}{\mathrm{d}t} = k_3 \times [\mathrm{Grb2}^*][\mathrm{Dvl}] - d_3 \times [\mathrm{Grb2\_Dvl}] \quad (13)$$

$$\frac{\mathrm{d}[\mathrm{Rac}^*]}{\mathrm{d}t} = k_4 \times [\mathrm{Grb2\_Dvl}][\mathrm{Rac}] - d_4 \times [\mathrm{Rac}^*] \quad (14)$$

$$\frac{\mathrm{d}[\mathrm{JNK}^*]}{\mathrm{d}t} = k_5 \times [\mathrm{Rac}^*][\mathrm{JNK}] - d_5 \times [\mathrm{JNK}^*] \quad (15)$$

$$\frac{\mathrm{d}[\mathrm{B}]}{\mathrm{d}t} = -k_6 \times [\mathrm{B}] \times [\mathrm{JNK}^*] - d_6 \times [\mathrm{B}] + \beta_6 + k_9 \times [\mathrm{E}\beta] - k_8 \times [\mathrm{B}] \times [E_\mathrm{m}] \quad (16)$$

$$\frac{d[E_c]}{dt} = k_9 \times [E\beta] - k_7 \times [E_c] \times \frac{E_m \times \beta}{33} + k_{10} \times [E_m] \times [E\beta] \quad (17)$$

$$\frac{d[E_m]}{dt} = k_7 \times [E_c] \times \frac{E_m \times \beta}{33} - k_8 \times [B] \times [E_m] - k_{10} \times [E_m] \times [E\beta] \quad (18)$$

$$\frac{d[E\beta]}{dt} = k_8 \times [B] \times [E_m] - k_9 \times [E\beta] \quad (19)$$

Note that protein degradation was also taken into account in these equations.

Initial protein concentrations and reaction constants

For simulating a wide range of ligand densities (LD), the ligand concentration was varied between 1 and 100 mM. Initial concentrations of β-catenin and E-cadherin were chosen similar to those reported in the literature.[5] Since, in our simulations, the total E-cadherin is distributed between the cytoplasmic pool (E_c), the membrane-localized pool (E_m) and in Eβ-complexes, for simplification, we have assumed equal concentrations of E_c, E_m and Eβ at the beginning of the simulations. The initial concentrations of FAK, GRB2 and DVL were calculated based on the stoichiometry relative to β-catenin reported in Crampton *et al.*[24] The initial concentrations of Rac and JNK, determined after multiple simulation runs, were chosen to be 10 nM, so as to obtain global steady state. For calculating the initial concentrations of phosphorylated forms of proteins, the ratio of non-phosphorylated form to phosphorylated form was chosen as 10 for all proteins. The value of GRB2_DVL was set equal to the value of GRB2*. Further, as done in the literature, to omit inclusion of conservation equations,[37] the cell was assumed to produce saturating levels of FAK, Grb2, Rac, Dvl and JNK, and hence the concentrations of these proteins were kept constant. Finally, though the initial value of E_c was kept constant in most of the simulations, the E_c values were changed in simulations to study the compensatory effect of E-cadherin upregulation on ligand density-mediated EMT (Fig. 4B).

The values of the kinetic constants are given in Table 2. Wherever possible, the values were chosen from the literature. If not available in the literature, the values were taken close to the related parameter values and considered such that a global steady state was reached. Values of C, k_1 and d_1 were chosen so as to ensure saturation in levels of FAK* for LD $\geq$ 50[36] and to get a global solution of the system of ODEs. Since Grb2 is known to activate Rac *via* the SH2 domain,[24] the values of k_3 were taken to be equal to the value of $k_{\_GS}$ in ref. 38. The value of parameter k_4 was determined from ref. 41. Since cancer cells have been reported to have a higher β-catenin production rate,[42] compared to the other rates, a higher value was considered for β-catenin production (1.98 nM s^{-1}). Further, we have multiplied the rate of translocation of E_c to E_m (*i.e.* k_7) by $\frac{E_m \times \beta}{33\ \text{nM}}$ to increase the translocation rate as the rate of Eβ formation increases (which depends on $E_m \times \beta$). Here 33 is just a scaling factor which was selected by running multiple simulations (data not shown).

Table 1 Initial concentrations of model species

Protein	Initial Conc.	Ref.
Ligand (LD)	1–100 mM	This paper
Grb2_Dvl (GD_0)	5.3 nM	This paper
FAK (F_0)	44 nM	5 and 24
FAK* (F_0*)	4.4 nM	This paper
GRB2 (G_0)	53 nM	5 and 24
GRB2* (G_0*)	5.3 nM	This paper
RAC (R_0)	10 nM	This paper
RAC* (R_0*)	1 nM	This paper
JNK (J_0)	10 nM	This paper
JNK* (J_0*)	1 nM	This paper
B (B_0)	33 nM	5 and 24
DVL (Dvl_0)	13 nM	5 and 24
E_m (E_{m0})	33 nM	5 and 24
E_c (E_{c0}), Eβ ($E\beta_0$)	33 nM	5 and 24

Similarly the rate of translocation of E_m to E_c (*i.e.* k_{10}) was multiplied by Eβ to increase the translocation rate as concentration of Eβ increases.

Model non-dimensionalization

The system of coupled ODEs (11) to (19) was non-dimensionalized. To obtain the dimensionless parameters, time (*i.e.* t) was rescaled with τ = 1 s and all protein levels by their respective initial concentrations (Table 1). Thus, the dimensionless model was obtained by setting,

$$\overline{\text{FAK}} = \frac{\text{FAK}}{F_0}, \overline{\text{FAK*}} = \frac{\text{FAK*}}{F_0^*}, \bar{t} = \frac{t}{\tau}, \overline{\text{Grb2}} = \frac{\text{Grb2}}{G_0},$$

$$\overline{\text{Grb2}^*} = \frac{\text{Grb2}}{G_0^*}, \overline{\text{Grb2\_Dvl}} = \frac{\text{Grb2\_Dvl}}{\text{GD}_0}, \overline{\text{Dvl}} = \frac{\text{Dvl}}{\text{Dvl}_0},$$

$$\overline{\text{Rac}} = \frac{\text{Rac}}{R_0}, \overline{\text{Rac}^*} = \frac{\text{Rac}^*}{R_0^*}, \overline{\text{JNK}} = \frac{\text{JNK}}{J_0}, \overline{\text{JNK*}} = \frac{\text{JNK*}}{J_0^*},$$

$$\bar{\beta} = \frac{\beta}{\beta_0}, \overline{E_m} = \frac{E_m}{E_{m0}}, \overline{E_c} = \frac{E_c}{E_{c0}}, \overline{E\beta} = \frac{E\beta}{E\beta_0}$$

After substituting these expressions in (11)–(19) and removing the overbars for simplicity, the following system of ODEs with dimensionless parameters were obtained:

Table 2 Kinetic constants and degradation rates

S.no.	Parameter	Value	Ref.
1	C	10 mM	Based on ref. 36
2	k_1	0.01 s^{-1}	Based on ref. 36
3	d_1	0.04 s^{-1}	Based on ref. 36
4	k_2	0.015 nM^{-1} s^{-1}	This paper
5	k_3	0.03 nM^{-1} s^{-1}	Based on ref. 38
6	d_3	0.9 s^{-1}	This paper
7	k_4	0.003 nM^{-1} s^{-1}	Based on ref. 39
8	d_4	0.0018 s^{-1}	Based on ref. 40
9	k_5	0.0055 nM^{-1} s^{-1}	This paper
10	d_5	0.003 s^{-1}	This paper
11	k_6	5.1 × 10^{-5} nM^{-1} s^{-1}	Unpublished reference
12	d_6	5 × 10^{-4} s^{-1}	Based on ref. 5
13	β_6	1.98 nM s^{-1}	This paper
14	k_7	3.3 nM^{-1} s^{-1}	Based on ref. 5
15	k_8	1.7 nM^{-1} s^{-1}	Based on ref. 5
16	k_9	3.3 s^{-1}	Based on ref. 5
17	k_{10}	3.3 nM^{-1} s^{-1}	Taken as equal to k_7

$$\frac{d[FAK^*]}{dt} = \hat{k}_1 \times \frac{[LD]}{C + [LD]} \times [FAK] - \hat{d}_1 \times [FAK^*] \quad (20)$$

$$\frac{d[Grb2^*]}{dt} = \hat{k}_2 \times [FAK^*][Grb2] - \hat{k}_3 \times [Grb2^*] \times [Dvl] \quad (21)$$

$$\frac{d[Grb2\_Dvl]}{dt} = \hat{k}_{11} \times [Grb2^*][Dvl] - \hat{d}_3 \times [Grb2\_Dvl] \quad (22)$$

$$\frac{d[Rac^*]}{dt} = \hat{k}_4 \times [Grb2\_Dvl][Rac] - \hat{d}_4 \times [Rac^*] \quad (23)$$

$$\frac{d[JNK^*]}{dt} = \hat{k}_5 \times [Rac^*][JNK] - \hat{d}_5 \times [JNK^*] \quad (24)$$

$$\frac{d[B]}{dt} = -\hat{k}_6 \times [B] \times [JNK^*] - \hat{d}_6 \times [B] + \hat{\beta}_6 + \hat{k}_9 \times [E\beta] - \hat{k}_8 \times [B] \times [E_m] \quad (25)$$

$$\frac{d[E_c]}{dt} = \hat{k}_{12} \times [E\beta] - \hat{k}_7 \times [E_c] \times \frac{E_m \times \beta}{33} + \hat{k}_{10} \times [E_m] \times [E\beta] \quad (26)$$

$$\frac{d[E_m]}{dt} = \hat{k}_{13} \times [E_c] \times \frac{E_m \times \beta}{33} - \hat{k}_{14} \times [B] \times [E_m] - \hat{k}_{15} \times [E_m][E\beta] \quad (27)$$

$$\frac{d[E\beta]}{dt} = \hat{k}_{16} \times [B] \times [E_m] - \hat{k}_{17} \times [E\beta] \quad (28)$$

where,

$$\hat{k}_1 = k_1 \times \tau \times \frac{F_0}{F_0^*};$$

$$\hat{k}_2 = k_2 \times \tau \times F_0^* \times \frac{G_0}{G_0^*};$$

$$\hat{k}_3 = k_3 \times \tau \times Dvl_0;$$

$$\hat{k}_4 = k_4 \times \tau \times GD_0 \times \frac{R_0}{R_0^*};$$

$$\hat{k}_5 = k_5 \times \tau \times R_0^* \times \frac{J_0}{J_0^*};$$

$$\hat{k}_6 = k_6 \times \tau \times J_0^*;$$

$$\hat{k}_7 = k_7 \times \frac{E_{m0} \times \beta_0 \times \tau}{33};$$

$$\hat{k}_8 = k_8 \times E_{m0} \times \tau;$$

$$\hat{k}_9 = k_9 \times \tau \times \frac{E\beta_0}{\beta_0};$$

$$\hat{k}_{10} = k_{10} \times \tau \times \frac{E_{m0}}{E_{c0}} \times E\beta_0;$$

$$\hat{k}_{11} = k_3 \times \frac{G_0^* \times Dvl_0}{(GD_0)} \times \tau;$$

$$\hat{k}_{12} = k_9 \times \tau \times \frac{E\beta_0}{E_{c0}};$$

$$\hat{k}_{13} = k_7 \times \frac{E_{c0} \times \beta_0 \times \tau}{33};$$

$$\hat{k}_{14} = k_8 \times \beta_0 \times \tau;$$

$$\hat{k}_{15} = k_{10} \times E\beta_0 \times \tau;$$

$$\hat{k}_{16} = k_8 \times \tau \times \beta_0 \times \frac{E_{m0}}{E\beta_0};$$

$$\hat{k}_{17} = k_9 \times \tau;$$

$$\hat{d}_i = d_i \times \tau \text{ for } i = 1, 3, 4, 5, 6;$$

The system of coupled dimensionless ODEs was then solved using the ode15s solver of Matlab subject to the conditions stated above. To confirm the correctness of solution of the ODE-based model, the network was also simulated using the SimBiology toolbox of Matlab, and the results were compared. For solving the model the 'sundials solver' with an absolute tolerance of 1×10^{-6} and a relative tolerance of 1×10^{-3} was used. A model was simulated for 10 000 time steps in SimBiology to achieve steady state levels of [Eβ].

Cellular automata-based hybrid model for population of cells

For incorporating the effect of cell–cell crosstalk in the model of ECM density-dependent regulation of cell–cell adhesion, a cellular automata-like hybrid model was developed in which the concentrations of proteins were considered as continuous quantities (unlike pure automata where each cell can attain only discrete states) with each cell being represented as a discrete entity. The details of the hybrid cellular automaton model are as follows:

(1) *Geometry*: The model consisted of 100 cells arranged in a square lattice of 10 rows by 10 columns (Fig. 2A).

(2) *Geometry of the neighbourhood and boundary conditions*: To implement the neighbourhood, a von-Neuman-based interaction model was used where, in 2D, the future state of a cell was dependent on the states of four neighbouring cells (Fig. 2B). Periodic boundary conditions were imposed along the four edges of the lattice, *i.e.*, the last (first) cell in any row (or column) was considered to be adjacent to the first (last) cell in that row (column) (Fig. 2C).

(3) *States*: Each state 'S' of a cell was associated with the values of E_c, E_m, Eβ and B, respectively, *i.e.*, S ≡ (E_c, E_m, Eβ, and B), where E_c, E_m, Eβ and B represent the concentrations of cytoplasmic E-cadherin, membrane-bound E-cadherin, Eβ complex and non-phosphorylated β-catenin, respectively.

(4) *State transition rules*: To calculate the next state S_{new} of a cell, first the values of E_c, E_m, Eβ and B were updated for every cell *in parallel* based on the value of the ligand density and the current state. An earlier computational study has demonstrated that a single cell with weak cell–cell adhesion in an epithelial sheet is capable of inducing detachment in neighbouring cells.[5] For incorporating similar cell–cell interactions into our model, the Eβ value of each cell (*i.e.*, $E\beta_{i,j}^{n+1}$) was updated by setting it as the average of its own

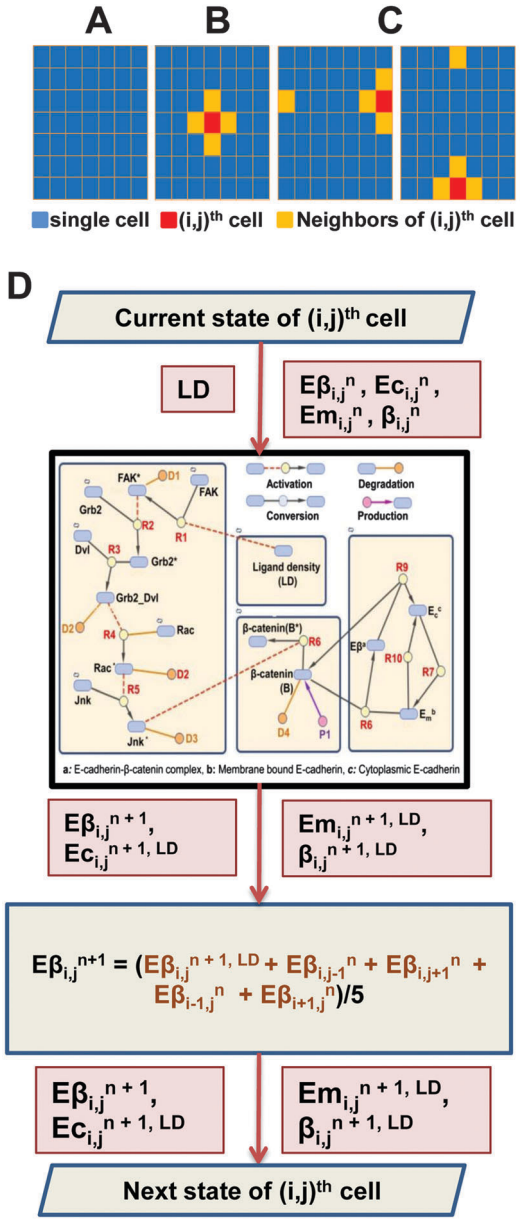

Fig. 2 Population model for studying the influence of ECM density on cell–cell adhesion. (A) Geometry of the population. The population consisted of 100 cells arranged in 10 rows and 10 columns. (B) Eβ levels of any given cell (shown in red colour) are dictated by its underlying ligand density and the Eβ levels of its four orthogonal neighbours (shown in orange colour). (C) Periodic boundary conditions were imposed along the four edges, *i.e.*, the last cell of any row (or any column) was assumed to be adjacent to the first cell of that row (column). (D) An algorithm for calculating Eβ levels of any given cell in the population. For taking both cell–matrix and cell–cell interactions into account, the Eβ level of each cell was updated by setting it as the average of its own value arising due to its interaction with its underlying matrix, and the Eβ values of its four neighbours (refer to Methods for details).

value arising due to its interaction with its underlying ligand (*i.e.*, $E\beta_{i,j}^{n+1,LD}$) and the Eβ values of its four neighbours $\left(i.e., E\beta_{i,j}^{n+1} = \frac{E\beta_{i,j}^{n+1,LD} + E\beta_{i,j-1}^{n} + E\beta_{i,j+1}^{n} + E\beta_{i-1,j}^{n} + E\beta_{i+1,j}^{n}}{5}\right)$ (Fig. 2D).

Experimental methods

ECM coating and cell culture. Ethanol sterilized glass coverslips were incubated with rat-tail collagen I (Sigma) at densities of 0.1, 1, and 10 μg cm^{-2} overnight in the refrigerator. Next day, the coverslips were washed with PBS and blocked with 2% F127 Pluronic (Sigma) for 10 min at room temperature. MCF-7 human breast cancer cells were cultured at 37° in DMEM (Dulbecco's Modified Eagle Medium) (Gibco) supplemented with 10% FBS (Gibco) and 1% antibiotics (Himedia). For experiments, equal number of cells were plated on ECM-coated glass coverslips and cultured for 24 hours.

Immunocytochemistry and microscopy. For E-cadherin staining, MDA-MB-231 and MCF-7 breast cancer cells were seeded on 12 mm collagen-coated coverslips at densities of 5×10^{-3} and 5×10^{-6} cells, respectively. After 24 h of incubation, cells were fixed with 4% paraformaldehyde (PFA) in 1× phosphate buffered saline (PBS) for 20 min. Subsequently, cells were blocked with 2% bovine serum albumin (BSA) solution for 45 min, and incubated with anti-E-cadherin rabbit polyclonal antibody (Abcam, Cat No: ab53033) at 1 : 100 dilution for one hour at room temperature (RT). After extensive washing with 1× PBS, cells were incubated with Alexa Fluor 555 conjugated anti-rabbit secondary antibody (Invitrogen) at 1 : 300 dilution for one hour at RT. Finally, cells were washed with 1× PBS twice and mounted on glass coverslips using Eukit mounting medium (Sigma). Mounted samples were imaged at 10× magnification on an inverted microscope (Olympus IX71) with a CCD camera (QImaging) using Image-Pro Express 6.3 acquisition software (Media Cybernetics). For analysis of ECM density-dependent E-cadherin localization, atleast 50 cells were analyzed per condition per experiment and the experiment repeated twice. Statistical significance was evaluated using Student's *t* test.

3 Results and discussion

Modulation of Eβ levels in a single cell by ECM density

Several studies have demonstrated a close connection between cell–cell adhesion and cell–matrix adhesion. Existing experimental data show that integrin-mediated cell–ECM adhesion inhibits cadherin mediated cell–cell adhesion.[21–23,43,44] To computationally probe the influence of ECM density on the non-dimensionalized Eβ levels in a single cell, the above model (Fig. 1) was simulated for ECM densities (LD) of 1, 3, 5 10, 20 and 50 mM, respectively, and the corresponding values of Eβ obtained. Initial protein levels are provided in Table 1 and discussed in the Methods section. Next, the system of ODEs (eqn 20–28) were solved subject to the above initial conditions to determine the transient profiles of Eβ levels.

The transient dynamics as well as steady-state values of the Eβ complex were strongly influenced by ECM density, with a decrease in the steady-state Eβ levels with increase in ligand density. The steady-state Eβ values for LD = 1 and LD = 50 were 2.0 and 0.78, respectively (Fig. 3A). Identical results were also obtained from the Simbiology-based model. To further quantify the ligand density-dependent modulation of Eβ levels,

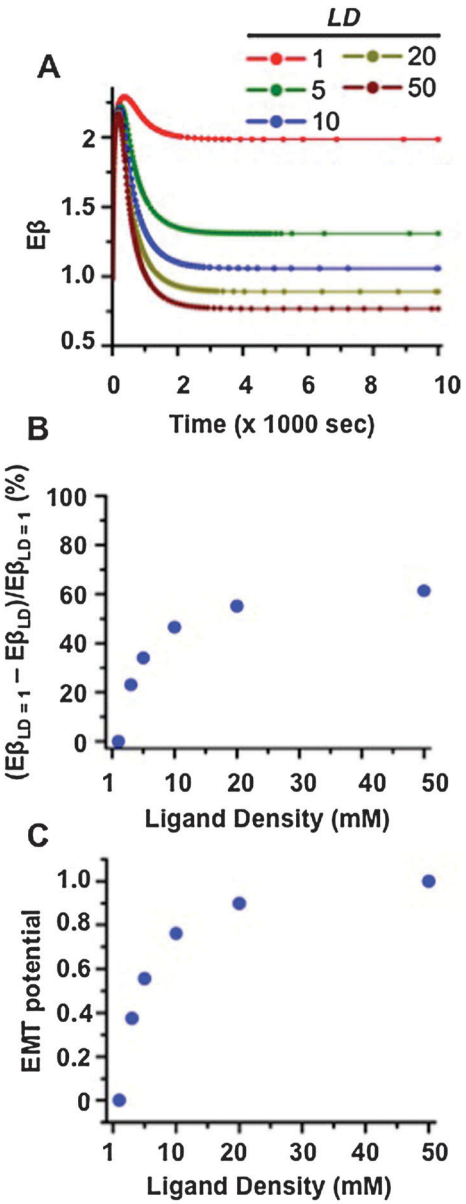

Fig. 3 Influence of ECM density on Eβ levels in a single cell. (A) Temporal dynamics of Eβ levels (normalized w.r.t. initial concentration) in a single cell at varying ligand densities. Eβ levels were allowed to evolve till a steady-state was reached. (B) Percentage reduction in Eβ values at varying ligand densities. The percentage reduction was calculated taking $E\beta_{LD=1}$ as a reference. (C) EMT potential was calculated by normalizing the percentage reduction in Eβ values w.r.t the maximal reduction observed at the highest ligand density. Thus EMT potential was zero at LD = 1 and one at LD = 50.

the percentage reduction in Eβ levels was calculated for varying values of ligand density considering the steady-state value of Eβ at LD = 1 as reference (Fig. 3B). The percentage reduction in Eβ levels exhibited a ligand density-dependent saturation profile with saturation levels reached for LD $\geq$ 20. Since EMT is associated with loss of the Eβ complex from the cell membrane, therefore, to establish a relationship between ligand density and EMT potential of a cell, the percentage reduction in Eβ levels with increasing ligand density obtained above was normalized so that maximal EMT potential was associated with the highest density surfaces (Fig. 3C).

Effect of E-cadherin overexpression on Eβ levels in a single cell

Several experimental studies have demonstrated that EMT involves repression of E-cadherin expression[7,8,45,46] and that EMT can be suppressed by overexpressing E-cadherin.[47–49] To test if similar results can be obtained within this computational framework, Eβ levels were computed after increasing E-cadherin levels (E_c) for different values of ligand densities. For implementing this in the simulations, Eβ levels on a given ligand surface were allowed to reach steady-state, at which point the value of E_c was instantaneously increased and the new value of Eβ determined. The value of E_c was increased in multiples of $E_{c,LD=1}$ at steady state (*i.e.*, the steady state concentration of E_c at LD = 1). As observed in Fig. 4A, a $3 \times E_{c,LD=1}$ increase in E_c led to a corresponding increase in Eβ values depending on ligand density, highlighting the positive influence of E-cadherin in suppressing EMT. However, as is clear from the E-cadherin profiles, the overexpression has less of an effect at higher ligand densities.

The above simulations were performed only for three ligand densities corresponding to a $3 \times E_{c,LD=1}$ increase in E-cadherin levels. Since the net increase in Eβ levels is dependent both on the extent of E-cadherin overexpression and the ligand density, therefore to fully explore the parameter space, simulations were performed for several combinations of ligand densities and the amount of E-cadherin overexpression. Specifically, simulations were performed to analyse the effect of increasing E_c levels by an amount of $k \times E_{c,LD=1}$, where k was varied from 0 (corresponding to no increase) to 15. Interestingly, the fold-change in Eβ levels scaled linearly with the fold-change in E-cadherin levels across all ligand densities (Fig. 4B).

In addition to illustrating the opposing effects of E-cadherin and ligand density on Eβ levels in a single cell (Fig. 4A and B), these results indicate that increase in ligand density can be counterbalanced by increase in E-cadherin levels. To quantitatively establish the nature of this relationship, ligand density was increased from LD = 1 (chosen as reference) to higher values, and the increase in E-cadherin determined to keep the Eβ value the same as the value corresponding to LD = 1 and $E_{c,LD=1}$. As observed in Fig. 4C, the increase in E-cadherin levels required for counterbalancing the effect of ligand density exhibited a sigmoidal dependence on ligand density (Fig. 4C). Saturation was observed for LD $\geq$ 50, with a five-fold increase in E-cadherin levels.

Modulation of Eβ levels by ECM density at the population level

Though insightful, in the above simulations, Eβ dynamics in single cells were computed for varying ECM density and E-cadherin without considering the effect of cell–cell adhesion. To study ECM density-dependent Eβ dynamics in a population of cells, a cellular automata-like hybrid model was developed where cells were considered as discrete entities and concentration of proteins as continuous quantities (Fig. 2). For incorporating cell–cell crosstalk in our model, a simple averaging

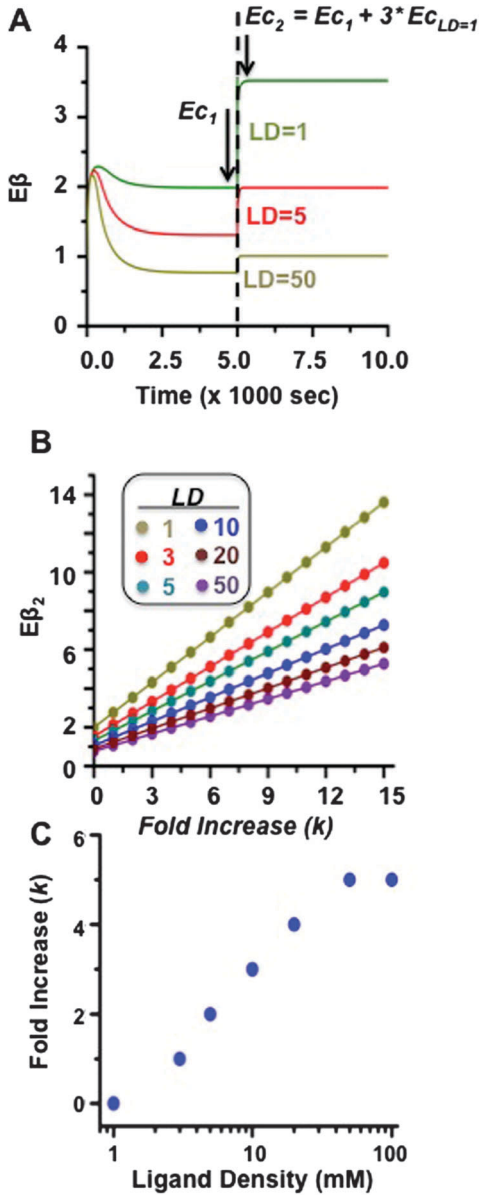

Fig. 4 Influence of E-cadherin overexpression on Eβ levels in a single cell. (A) ECM density-dependent Eβ dynamics was tracked at different ligand densities. When steady-state levels were reached, E-cadherin levels were increased by 3 × $E_{c,LD=1}$ and new Eβ levels determined. (B) New Eβ levels ($Eβ_2$) reached for different extents of E-cadherin overexpression (*i.e.*, *k*). (C) Fold change in E-cadherin levels required to nullify the effect of ECM density, *i.e.*, to ensure $Eβ_2 = Eβ_{LD=1}$.

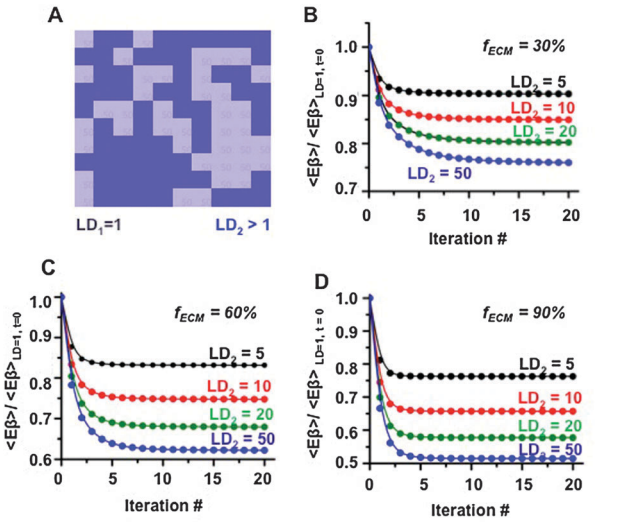

Fig. 5 Influence of heterogeneously distributed ECM on population-level Eβ dynamics. (A) Eβ values of all cells were initialized to $Eβ_{LD=1}$. Simulations were performed by increasing the ligand density from LD_1 = 1 (light blue regions) in a certain fraction of the ECM (f_{ECM}) to higher values of the ligand density ($LD_2 \geq 5$) (deep blue regions), and the population-averaged Eβ level (*i.e.*, ⟨Eβ⟩) was tracked. The value was normalized w.r.t the initial value (*i.e.*, $\langle Eβ \rangle_{t=0}$). The portions of different ligand densities were randomly chosen based on the value of f_{ECM}. (B–D) Temporal dynamics of normalized ⟨Eβ⟩ levels for f_{ECM} = 30, 60 and 90%, respectively, and LD_2 = 5, 10, 20 and 50, respectively.

approach was used where, at every simulation step, the Eβ levels of every cell were updated by setting it as the average of its own value based on cell–matrix interactions (calculated above in Fig. 2) and that of its four orthogonal neighbours (Fig. 2B–D). Periodic boundary conditions were used to compute the average for cells located along any one of the four edges (Fig. 2C).

When a uniform ligand density was chosen, the steady-state Eβ levels were identical to the values obtained for single cells without taking cell–cell interactions into account (data not shown).

In vivo, ECM density can be highly heterogeneous both in composition and in density. To explore the influence of heterogeneity in ECM density on population-level Eβ dynamics, simulations were performed by increasing the ligand density from LD = 1 in a certain fraction of the ECM (f_{ECM} = 30,60,90%) to higher values of ligand density (LD ≥ 5) (Fig. 5A). As observed in Fig. 5B–D, increase in ligand density from LD = 1 to LD ≥ 5 led to a corresponding decrease in the steady-state Eβ levels, with progressively lower values observed at higher ECM densities. Further, the drop in Eβ levels was higher for higher values of f_{ECM}. Greater than 25% reduction in Eβ levels was observed when the ligand density was increased at least 10-fold in greater than 60% of the ECM. Collectively, these results suggest that a significant increase in local ligand density is required to elicit global population-level scattering.

Influence of EMT cells on scattering of a cell population

In the above simulations, all cells were assumed to be normal cells, and the scattering was induced purely by ligand density. It is conceivable that in a heterogeneous cell population containing cells which have already undergone EMT (referred to here as EMT cells), a single EMT cell can influence the Eβ levels of its neighbouring cells through cell–cell crosstalk. Such crosstalk has been shown to be capable of generating an EMT wave in the entire population.[5]

To study the influence of EMT cells on ECM density-dependent modulation of Eβ levels at the population level, simulations were performed for varying fractions of 'EMT cells (f_{EMT}) placed randomly in a population of 100 cells (Fig. 6A).

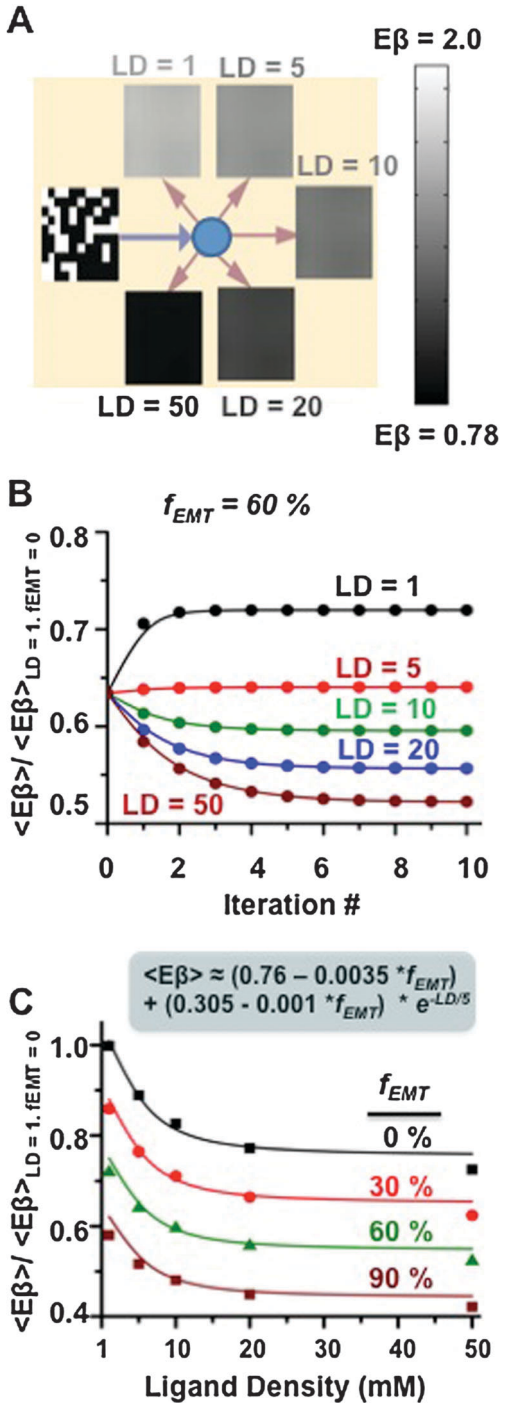

Fig. 6 Influence of EMT cells on population-level scattering. (A) Simulations were performed assuming that a certain fraction of cells (f_{EMT}) were EMT cells (black) and the remaining were normal cells (white). Eβ levels of normal cells were initialized to $E\beta_{LD=1}$ and that of EMT cells intialized to $E\beta_{LD=50}$. As before, the population-averaged Eβ level ($\langle E\beta \rangle$) was tracked till a steady-state was reached. (B) Temporal dynamics of $\langle E\beta \rangle$ (normalized w.r.t. $\langle E\beta \rangle_{LD=1,f_{EMT}=0\%}$) at different ligand densities for f_{EMT} = 60%. (C) Steady-state $\langle E\beta \rangle$ levels at varying ECM densities and varying f_{EMT} fractions. Lines represent a fit to the equation $\langle \bar{E}\bar{\beta} \rangle = (0.76 - 0.0035 f_{EMT}) + (0.305 - 0.001 f_{EMT}) e^{-LD/5}$.

While cells with $E\beta \geq E\beta_{LD=1}$ were assumed to be normal cells, cells with $E\beta \leq E\beta_{LD=50}$ were labeled as EMT cells. Eβ values for EMT cells were initialized to 0.78 (*i.e.*, $E\beta_{LD=50}$ normalized w.r.t. the initial concentration), and the Eβ values for non-EMT cells were initialized to 2 (*i.e.*, $E\beta_{LD=1}$) (see Fig. 3A). As before, the evolution of Eβ values for the entire population was dependent on ligand density. Fig. 6B shows the transient evolution of population-averaged Eβ levels at different ligand densities assuming 60% EMT cells in the population. The population-averaged value was normalized w.r.t. $E\beta_{LD=1}$ and f_{EMT} = 0% yielding a value of $\left(\frac{(2 \times 40 + 0.78 \times 60)/100}{2}\right) = 0.634$ at the start of the simulations. Interestingly, the steady-state population-averaged Eβ values increased at lower ligand densities (LD $\leq$ 5), remained nearly constant for LD = 5, and decreased at higher ligand densities. These results indicate that EMT can be suppressed at moderate to low ligand densities even in the presence of sizeable population of EMT cells. Near identical results were obtained when all the EMT cells were localized in the centre of the population, indicating a negligible influence of the spatial location of EMT cells on cell scattering (data not shown).

To further quantify the ligand density-dependent modulation of Eβ levels in a heterogeneous cell population, the above simulations were performed for varying fractions of EMT cells (f_{EMT} = 0,30,60,90%), and the evolution of steady-state population-averaged Eβ levels (normalized to steady-state values reached at LD = 1 and f_{EMT} = 0%) was plotted for varying values of ligand density (Fig. 6C, Fig. S1, ESI†). While the nature of the curves remained the same, increasing the EMT fraction led to a near constant reduction in Eβ values across all the ligand densities. The simulated points were well fit with the expression $\langle \bar{E}\bar{\beta} \rangle = (0.76 - 0.0035 f_{EMT}) + (0.305 - 0.001 f_{EMT}) e^{-LD/5}$ highlighting the coupled influence of both ligand density and EMT fraction on population-level scattering.

Effect of E-cadherin overexpression on Eβ levels at the population level

Our previous simulations at the single cell level had demonstrated the ability of E-cadherin overexpression to counter the influence of ligand density in modulating Eβ expression. To probe how these results would get altered at the population level, simulations were performed using the hybrid model for a heterogeneous cell population with varying fractions of EMT cells (Fig. 7). In doing these simulations, similar to the single cell case, the population-averaged Eβ levels on a given ligand surface were allowed to reach steady-state, at which point the value of E_c was instantaneously increased and the new value of population-averaged Eβ value determined. Interestingly, in a population of normal cells (*i.e.*, f_{EMT} = 0%), overexpression of E-cadherin by an amount of $5 \times E_{c,LD=1}$ led to an increase in the Eβ levels at the population level at the lowest ligand density (LD = 1), was able to nearly eliminate the ligand density-induced reduction in Eβ levels on a moderately high ligand surface (LD = 10), and partly restored the Eβ levels at the highest ligand density (LD = 50) (Fig. 7A). However, for all the cases, the restoration of Eβ levels was more gradual compared to the near instantaneous increase observed for the single cell case.

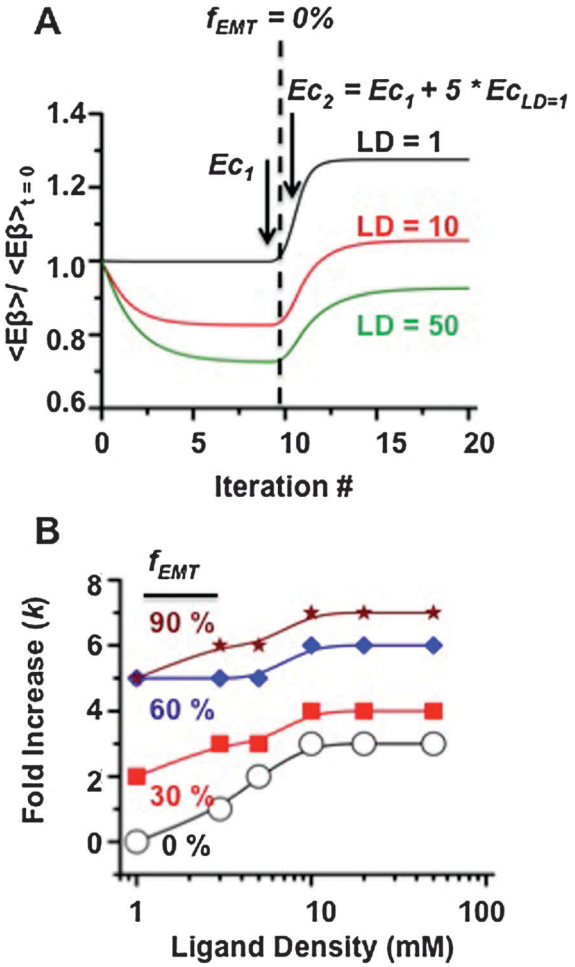

Fig. 7 Influence of E-cadherin overexpression on population level Eβ values. (A) ECM density-dependent ⟨Eβ⟩ dynamics was tracked at different ligand densities. When steady-state levels were reached, E-cadherin levels were increased by an amount of 5 × $E_{c,LD=1}$ and new ⟨Eβ⟩ levels determined. Eβ values were plotted by normalization w.r.t. steady-state ⟨Eβ⟩ levels reached at LD = 1 before over-expressing E-cadherin. (B) Required fold-change in E-cadherin levels required to nullify the effect of ECM density on Eβ levels for varying fractions of EMT cells (f_{EMT} = 0, 30, 60, 90%).

To further explore the crosstalk between E-cadherin overexpression and ECM density in a heterogeneous population containing EMT cells, the fraction of EMT cells was varied, ligand density was increased from LD = 1 (chosen as reference) to higher values, and the fold-change in E-cadherin levels (*i.e.*, the factor *k*) determined to keep population-averaged Eβ levels same as the value corresponding to LD = 1 and $E_{c,LD=1}$. The nature of the dependence of fold-change in E-cadherin on ligand density for a cell population was similar to that of single cells (Fig. 7B). Though, the requirement of E-cadherin increase on ligand density was higher when EMT cells were present, the nature of the dependence was found to be similar for different EMT fractions, with saturation observed for LD ≥ 10. Collectively, these results suggest that at the population level, the presence of EMT cells alters the sensitivity of E-cadherin increase in counterbalancing the effects of ECM density.

Effect of ECM density on E-cadherin localization patterns in human breast cancer cells

Thus far, our simulation results illustrate negative regulation of cell–cell adhesions by ECM density. As a final step, to compare our model predictions with the behavior of cancer cells, ECM density-dependent E-cadherin localization was quantified in MCF-7 and MDA-MB-231 human breast cancer cell lines. Specifically, the cytoplasmic/membrane localization pattern of E-cadherin was tracked in cells cultured on substrates coated with collagen at densities of 0.1, 1.0 and 10.0 μg cm^{-2}, respectively (Fig. 8). Cells were cultured for 24 hours and subsequently

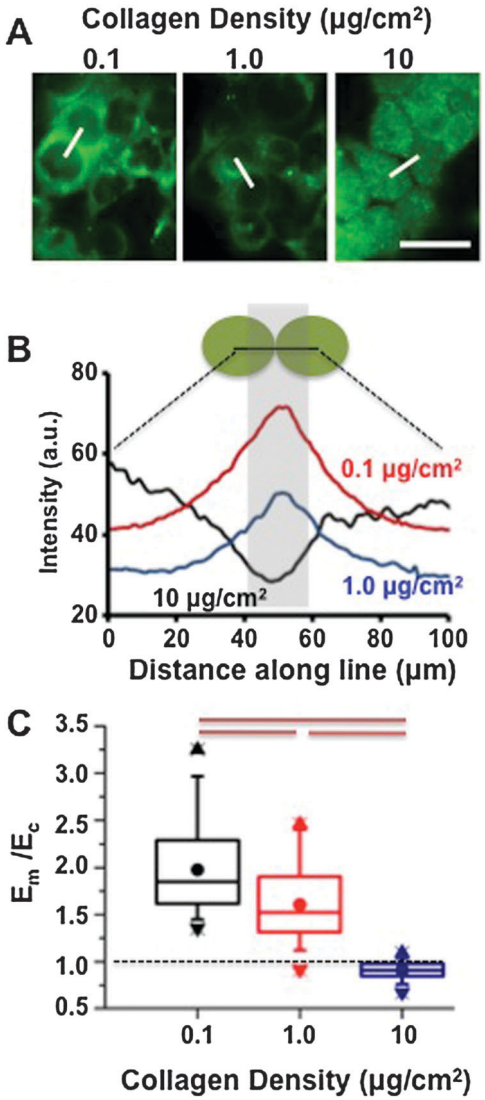

Fig. 8 ECM density-dependent E-cadherin localization patterns in MCF-7 human breast cancer cells. (A) MCF-7 cells were cultured on 0.1, 1.0 and 10 μg cm^{-2} collagen-coated coverslips for 24 hours. Representative images of MCF-7 cells cultured at different ECM densities stained with E-cadherin antibody. Scale bar = 50 μm. (B) Cells across different conditions were imaged under identical camera gain and exposure settings. Line intensities along lines drawn across cell–cell contacts at three different ECM densities (A, schematic). (C) Ratio of membrane to cytoplasmic E-cadherin levels (*i.e.*, E_m/E_c at varying ECM densities. Bars indicate statistical significance (*$p < 0.05$)).

fixed and stained to visualize the localization pattern of E-cadherin. While MCF-7 cells were plated at a high density to allow for cell–cell bonds to form, MDA-MB-231 cells were cultured sparsely. Consistent with model predictions, a distinct change in E-cadherin localization was observed with increasing collagen density in both cases.

In MCF-7 cells, in contrast to the lowest coating density, where cells maintained cell–cell contacts, at the highest coating density, E-cadherin was markedly absent at cell–cell contacts (Fig. 8A). To assess this quantitatively, the membrane *versus* cytoplasmic localization patterns of E-cadherin was determined across the different collagen densities by tracking E-cadherin intensity profiles along lines (white lines, Fig. 8A) connecting cells in contact and passing through the cell–cell junction (Fig. 8B, schematic). While E-cadherin exhibited a stronger localization at cell–cell contacts compared to the cytoplasm on the 0.1 μg cm^{-2} substrates as evidenced by the peak in the line intensity at the cell–cell junction, the localization pattern was exactly reversed on the 10.0 μg cm^{-2} substrate with a corresponding dip in the line intensity at the cell–cell junction (Fig. 8B). Tracking the membrane to cytoplasmic ratios (*i.e.*, E_m/E_c) for multiple cells revealed a significant drop from ≈ 2 observed on the lowest density surfaces to ≈ 0.75 on the highest density surfaces (Fig. 8C).

For MDA-MB-231 cells, which were grown under sparse conditions, differences were observed in the E-cadherin localization pattern, with highest E_m/E_c ratios observed at the lowest ECM density (Fig. S2, ESI†). Though these ratios were significantly less compared to the ratios observed in MCF-7 cells which formed cell–cell contacts, still the density-dependent differences were statistically significant. Collectively, these data are consistent with the model predictions and illustrate the strong influence of ECM density on the localization pattern of E-cadherin.

4 Discussion

Tissue homeostasis requires a fine balance between cell–cell and cell–matrix adhesions. In cancer, this balance is lost *via* disruption of cell–cell adhesions and formation of cell–matrix adhesions which induce cell migration and invasion. In this paper, we have developed a computational framework to probe the modulation of cell–cell adhesions by ECM density, which has been documented to increase during cancer progression. By tracking Eβ concentration as a metric of cell–cell adhesion, we have shown that both for single cells as well as for a cell population, Eβ levels negatively correlate with ligand density. Next, we have computationally shown that ECM density-induced down regulation in Eβ levels can be partly reversed by overexpression of E-cadherin. By simulating the dynamics of a heterogeneous cell population containing a fraction of EMT cells, we have demonstrated that the scattering tendency of the entire population is dictated collectively by ECM density and the fraction of EMT cells. Finally, consistent with our model predictions, we have demonstrated a re-localization of E-cadherin from cell–cell contacts to the cytoplasm in MCF-7 cells at higher ECM densities. Taken together, our results illustrate how increase in ECM density can directly contribute to EMT through dissociation of cell–cell adhesions.

In vivo, epithelial cells are in contact with both the underlying ECM as well as with neighbouring cells. While cell–matrix adhesions are mostly integrin-based, cell–cell adhesion is primarily mediated by cadherins. Several experimental studies support the idea of a crosstalk between the two adhesion apparatus, with examples of both positive[16,50] as well as negative crosstalk[17,18,21] being observed. Though the exact mechanisms are not fully understood, the non-receptor tyrosine kinase FAK represents an important link between the two types of structures. Here, we have explored the crosstalk between cell–cell and cell–matrix adhesions *via* the pathway linking integrin engagement with the ECM ligand, FAK activation and FAK mediated phosphorylation of β-catenin through Grb2, Dvl, Rac and JNK.[6,24,25] Simulation of the above network has highlighted the role of this signaling cascade in negatively regulating the strength of cell–cell adhesions.[21,51] Our results suggest that increase in ECM density can promote EMT by weakening cell–cell adhesions even in the absence of the EMT activator TGFβ. This was also observed experimentally in MCF-7 human breast cancer cells cultured on collagen-coated surfaces of increasing density, where increase in ECM density led to a significant drop in the ratio of membrane-localization to cytoplasmic E-cadherin.

Within EMT, the epithelial and mesenchymal cells represent the two extremes of the transition process. Given the huge heterogeneity that exists in a tumor, it is likely that intermediate phenotypes exist which correspond to partial EMT states. Such intermediate states have been described during wound healing,[52] migration of neural crest cells,[53] in liver epithelial cells,[54] and in carcinosarcomas.[55] The stability of such a mixed population and sensitivity to ECM density remains unknown. To answer this, we have tracked ECM density-induced population scattering tendency for a mixed population containing varying fractions of cells that have already undergone EMT (*i.e.*, have low Eβ levels). Surprisingly, our results suggest that the EMT phenotype can be partly reversed at low ECM densities (*e.g.*, LD = 1), as evidenced by the increase in Eβ levels. Furthermore, our results are indicative of a combined influence of EMT cells and ECM density on population-level scattering. For a given fraction of EMT cells, the nature of dependency of Eβ levels on ligand density remained nearly identical with no difference observed for LD $\geq$ 20, suggesting a certain range (1 $\leq$ LD $\leq$ 20) within which EMT can be driven by ECM density alone. Increase in the EMT fraction led to a near constant drop in Eβ levels that was independent of ligand density. Such change in the fraction of EMT cells may arise from soluble factors like TGFβ. Our results also indicate that localized induction of EMT signals and randomly distributed EMT signals have similar effects on population-averaged Eβ levels. Collectively, these results indicate that EMT can be induced by a combination of ECM-based cues that alter ECM density or soluble and/or other cues that alter the fraction of EMT cells.

Suppression of EMT by direct/indirect increase in E-cadherin expression levels has been demonstrated by several experimental studies.[47–49] However, given the crosstalk between cell–cell and cell–matrix adhesions, it is likely that the extent of EMT reversal by E-cadherin expression is influenced by ECM density. We have addressed this question by determining the level of E-cadherin increase required to outweigh ECM density-induced reduction in Eβ levels. Our simulations clearly demonstrate that the fold-change in E-cadherin levels required for reversing EMT is dependent on ECM density. For single cells in contact with the surrounding ECM, a two order of magnitude increase in ECM density was found to require a 5-fold increase in E-cadherin levels for maintaining constant Eβ levels. At the population level, the change in E-cadherin levels was dependent on ECM density as well as the fraction of EMT cells. Increase in E-cadherin levels saturated for LD $\geq$ 10 to 3-fold for 0% EMT cells and 7-fold for 90% EMT cells. Taken together, these results suggest that ECM density and the fraction of EMT cells collectively dictate the extent of E-cadherin overexpression required for EMT reversal.

5 Conclusions

The presented work demonstrates an intimate relationship between ECM density and cell–cell adhesions, both computationally and experimentally. Our results suggest that ECM density-induced down regulation in Eβ levels can be reversed effectively by overexpression of E-cadherin depending on ECM density and the fraction of EMT cells. Our results also illustrate that the scattering tendency of a heterogeneous cell population is dictated both by ECM density and the fraction of EMT cells. However, the spatial position of the EMT cells does not matter. Future work will be focused on extending the computational framework for studying the crosstalk between ECM density and other aspects of cancer invasion including extracellular proteolysis and collective cell invasion. Incorporation of biophysical interactions between individual cells and with their matrix is expected to provide further insight into these processes.

Acknowledgements

We acknowledge financial support from the IIT Bombay Seed Grant for carrying out this work. AD was supported by funding from DBT.

References

1 M. A. Nieto, *Annu. Rev. Cell Dev. Biol.*, 2011, **27**, 347–376.
2 B. D. Craene and G. Berx, *Nat. Rev. Cancer*, 2013, **13**, 97–110.
3 K. Polyak and R. A. Weinberg, *Nat. Rev. Cancer*, 2009, **9**, 265–273.
4 J. Massague, *Cell*, 2008, **134**, 215–230.
5 I. Ramis-Conde, D. Drasdo, A. R. A. Anderson and M. A. J. Chaplain, *Biophys. J.*, 2008, **95**, 155–165.
6 M. H. Lee, P. Koria, J. Qu and S. T. Andreadis, *FASEB J.*, 2009, **09**, 3874–3883.
7 A. Cano, M. A. Perez-Moreno, I. Rodrigo, A. Locascio, M. J. Blanco, M. G. del Barrio, F. Portillo and M. A. Nieto, *Nat. Cell Biol.*, 2000, **2**, 76–83.
8 B. M. Gumbiner, *J. Cell Biol.*, 2000, **148**, 399–404.
9 P. P. Provenzano, K. W. Eliceiri, J. M. Campbell, D. R. Inman, J. G. White and P. J. Keely, *BMC Med.*, 2006, **4**(38), 1–16.
10 P. P. Provenzano, D. R. Inman, K. W. Eliceiri, J. G. Knittel, L. Yan, C. T. Rueden, J. G. White and P. J. Keely, *BMC Med.*, 2008, **6**(11), 38–230.
11 M. J. Paszek, N. Zahir, K. R. Johnson, J. N. Lakins, G. I. Rozenberg, A. Gefen, C. A. Reinhart-King, S. S. Margulies, M. Dembo, D. Boettiger, D. A. Hammer and V. M. Weaver, *Cancer Cell*, 2005, **8**(3), 241–254.
12 K. R. Levental, H. Yu, L. Kass, J. N. Lakins, M. Egeblad, J. T. Erier, S. F. Fong, K. Csiszar, A. Giaccia, W. Weninger, M. Yamaguchi, D. L. Gasser and V. M. Weaver, *Cell*, 2009, **139**(5), 891–906.
13 P. J. Wipff, D. B. Rifkin, J. J. Meister and B. Hinz, *J. Cell Biol.*, 2007, **179**(6), 1311–1323.
14 A. Das, A. Kapoor, G. D. Mehta, S. K. Ghosh and S. Sen, *J. Carcinog. Mutagen.*, 2013, DOI: 4172/2157-2518.S13-003.
15 M. Burute and M. Thery, *Curr. Opin. Cell Biol.*, 2012, **24**(5), 628–636.
16 M. R. Clara, F. Pincet, J. P. Thiery and S. Dufour, *J. Cell Sci.*, 2010, **123**(5), 712–722.
17 J. Tsai and L. Kam, *Biophys. J.*, 2009, **96**, 39–41.
18 G. K. Ojakian, D. R. Radcliffe and R. Schwimmer, *J. Cell Sci.*, 2000, **114**, 941–952.
19 O. V. Sazanova, K. L. Lee, B. C. Isenberg, C. B. Rich, M. A. Nugent and J. Y. Wong, *J. Cell Sci.*, 2000, **114**, 941–952.
20 C. S. Chen, J. Tan and J. Tien, *Annu. Rev. Biomed. Eng.*, 2004, **6**, 275–302.
21 J. de Rooij, A. Kerstens, G. Danuser, M. a. Schwartz and C. M. Waterman-Storer, *J. Cell Biol.*, 2005, **171**, 153–164.
22 T. Genda, M. Sakamoto, T. Ichida, H. Asakura and S. Hirohashi, *Lab. Invest.*, 2000, **80**, 387–394.
23 A. Koenig, C. Mueller, C. Hasel, G. Adler and A. Menke, *Cancer Res.*, 2006, **66**, 4662–4671.
24 S. P. Crampton, B. Wu, E. J. Park, J. H. Kim, C. Solomon, M. L. Waterman and C. C. W. Hughes, *PLoS One*, 2009, **4**, e7841.
25 X. Wu, X. Tu, K. S. Joeng, M. J. Hilton, D. A. Williams and F. Long, *Cell*, 2008, **133**, 340–353.
26 V. Quaranta, A. M. Weaver, P. T. Cummings and A. R. A. Anderson, *Clin. Chim. Acta*, 2005, **357**, 173–179.
27 H. M. Byrne, *Nat. Rev. Cancer*, 2010, **10**, 221–230.
28 K. Gammon, *Nature*, 2012, **491**, S66–S67.
29 N. Savage, *Nature*, 2012, **491**, S62–S63.
30 J. Moreira and A. Deutsch, *Adv. Complex Syst.*, 2002, **5**, 247–267.
31 T. Alarcón, H. M. Byrne and P. K. Maini, *J. Theor. Biol.*, 2003, **225**, 257–274.
32 H. Enderling, N. R. Alexander, E. S. Clark, K. M. Branch, L. Estrada, C. Crooke, J. Jourquin, N. Lobdell, M. H. Zaman, S. a. Guelcher, A. R. a. Anderson and A. M. Weaver, *Biophys. J.*, 2008, **95**, 2203–2218.

33 A. Q. Ninh, *Int. J. Biosci., Biochem. Bioinf.*, 2013, **3**, 5–8.
34 D. Basanta, D. W. Strand, R. B. Lukner, O. E. Franco, D. E. Cliffel, G. E. Ayala, S. W. Hayward and A. R. Anderson, *Cancer Res.*, 2009, **69**(17), 7111–7120.
35 E. Kim, V. Rebecca, I. V. Fedorenko, J. L. Messina, R. Mathew, S. Maria-Engler, D. Basanta, K. S. Smalley and A. R. Anderson, *Cancer Res.*, 2013, **73**, 6874–6885.
36 A. R. Asthagiri, C. M. Nelson, A. F. Horwitz and D. A. Lauffenburger, *J. Biol. Chem.*, 1999, **274**, 27119–27127.
37 A. Macdonald, A. R. Horwitz and D. A. Lauffenburger, *Cell Adh. Migr.*, 2008, **2**, 95–105.
38 A. Nag, M. Monine, A. S. Perelson and B. Goldstein, *PLoS One*, 2011, **7**(3), e28758.
39 J. Das, M. Ho, J. Zikherman, C. Govern, M. Yang, A. Weiss, A. K. Chakraborty and J. P. Roose, *Cell*, 2009, **136**, 337–351.
40 L. C. Haeusler, L. Hemsath, D. Fiegen, L. Blumenstein, U. Herbrand, P. Stege, R. Dvorsky and M. R. Ahmadian, *Methods Enzymol.*, 2006, **406**, 1–11.
41 T. S. Freedman, H. Sondermann, G. D. Friedland, T. Kortemme, D. Bar-Sagi, S. Marqusee and J. Kuriyan, *Proc. Natl. Acad. Sci. U. S. A.*, 2006, **103**, 16692–16697.
42 T. Utsunomiya, Y. Doki, H. Takemoto, H. Shiozaki, M. Yano, M. Sekimoto, S. Tamura, T. Yasuda, Y. Fujiwara and M. Monden, *Oncology*, 2001, **61**(3), 226–233.
43 E. Avizienyte, A. W. Wyke, R. J. Jones, G. W. McLean, M. A. Westhoff, V. G. Brunton and M. C. Frame, *Nat. Cell Biol.*, 2002, **4**, 632–638.
44 Y. Wang, G. Jin, H. Miao, J. Y. S. Li, S. Usami and S. Chien, *Proc. Natl. Acad. Sci. U. S. A.*, 2006, **103**, 1774–1779.
45 S. Hirohashi, *Am. J. Pathol.*, 1998, **153**, 333–339.
46 E. Batlle, E. Sancho, C. Franci, D. Dominguez, M. Monfar, J. Baulida and A. Garcia de Herreros, *Nat. Cell Biol.*, 2000, **2**, 84–89.
47 K. Vleminckx, L. Vakaet, M. Mareel, W. Fiers and F. van Roy, *Cell*, 1991, **66**, 107–119.
48 G. Christofori and H. Semb, *Trends Biochem. Sci.*, 1999, **24**, 73–76.
49 V. Tripathi, N. C. Popescu and D. B. Zimonjic, *Oncogene*, 2013, 1–10.
50 L. A. Trinh and D. Y. Stainier, *Dev. Cell*, 2004, **6**, 371–382.
51 Y. Shintani, M. J. Wheelock and K. R. Johnson, *Mol. Biol. Cell*, 2006, **17**, 2963–2975.
52 V. Arnoux, M. Nassour, A. L'Helgoualch, R. A. Hipskind and P. Savagner, *Mol. Biol. Cell*, 2008, **19**, 4738–4749.
53 E. Theveneau, L. Marchant, S. Kuriyama, M. Gull, B. Moepps, M. Parsons and R. Mayor, *Dev. Cell*, 2010, **19**(1), 39–53.
54 M. Zeisberg, C. Yang, M. Martino, M. B. Duncan, F. Rieder, H. Tanjore and R. Kalluri, *J. Biol. Chem.*, 2007, **282**(32), 32337–32347.
55 D. Sarrio, S. M. Rodriguez-Pinilla, D. Hardisson, A. Cano, G. Moreno-Bueno and J. Palacios, *Cancer Res.*, 2008, **68**, 989–997.